Defect and impurity properties of hexagonal boron nitride: A first-principles calculation

Bing Huang[1,*] and Hoonkyung Lee[2,†]
[1]*Department of Physics, Tsinghua University, Beijing 100084, China*
[2]*Division of Quantum Phases and Devices, School of Physics, Konkuk University, Seoul 143-701, Korea*
(Received 20 September 2012; published 7 December 2012)

In this paper, we have systematically studied the structural and electronic properties of vacancy defects and carbon impurity in hexagonal boron nitride (*h*-BN) by using both normal GGA calculations and advanced hybrid functional calculations. Our calculations show that the defect configurations and the local bond lengths around defects are sensitive to their charge states. The highest negative defect charge states are largely determined by the nearly-free-electron state at the conduction band minimum of BN. Generally, the in-gap defect levels obtained from hybrid functional calculations are much deeper than those obtained from normal GGA calculations. The formation energies of neutral defects calculated by hybrid functional and GGA are close to each other, but the defect transition energy levels are quite different between GGA and hybrid functional calculations. Finally, we show that the charged defect configurations as well as the transition energy levels exhibit interesting layer effects.

DOI: 10.1103/PhysRevB.86.245406 PACS number(s): 73.63.−b, 61.80.Fe, 61.82.Bg, 71.15.Mb

I. INTRODUCTION

Boron nitride (BN) has been investigated in great detail for a long time due to some of the fascinating properties, such as extreme hardness, high melting point, and wide band gap.[1] BN is known to have three different crystal structures: hexagonal BN (*h*-BN), cubic BN (*c*-BN), and wurzite BN (*w*-BN). Among these phases, *h*-BN is the stable one at room temperature and ambient pressure. Like the structure of graphite, *h*-BN consists of stacked BN layers with a honeycomb atomic network. Unlike semimetallic graphite, the ionic nature of B-N bond in *h*-BN results in a large band gap of around 6 eV,[2–5] making it an attractive candidate for optoelectronic applications in the ultraviolet energy range.[2,6]

Following the synthesis of graphene, single-layer and few-layers BN sheets are made in experiments by mechanical exfoliation,[7,8] controllable electron beam irradiation,[4,5] and chemical vapor deposition (CVD).[9–11] Various defects (e.g., vacancies[4,5]) and impurities (e.g., carbon and oxygen[8,10,11]) are observed in experiments during the synthesization of single-layer BN. Vacancies and C impurity have been demonstrated to have strong effects on the luminescence of BN based materials.[2,6,12,13] Thus, a full understanding of the properties of these defects and impurities in BN is of great importance for further optimizing its optical properties. Moreover, due to the similar atomic structures of BN and graphene, several attempts have been made to create the hybrid BNC structures by substitutional doping of C in BN structures during growth or postsynthesis.[14,15] BNC sheet has attracted great interests mainly due to its tunable band gap by controlling the relative concentration of C and BN. To further optimize the doping process in experiments, it is also important to understand the defect properties of C-doped BN. Although there are several calculations on the vacancy and impurity properties in BN,[16–23] a deep understanding of the neutral and charged defect structures, defect formation energies, defect levels, and the defect transition energy levels is still lacking, especially by the advanced hybrid functional calculations.

The aim of this paper is to give a full understanding of the properties of vacancy and C impurity in BN. Our calculations show that the defect configurations and the local bond lengths around defects are quite sensitive to their charge states. Interestingly, we find that the highest negative charge states of defects are largely determined by the nearly-free-electron (NFE) state at the conduction band minimum (CBM). After band gap correction, generally the in-gap defect levels obtained from hybrid functional calculations are quite deeper than those obtained from normal GGA calculations. The formation energies of neutral defects calculated by hybrid functional and GGA are close to each other, but the defect transition energy levels are quite different between GGA and hybrid functional calculations. Finally, we show that the charged defect configurations as well as the transition energy levels have interesting layer effects.

II. COMPUTATIONAL METHODS AND MODELS

Our calculations were performed by using density functional theory (DFT) in the generalized gradient approximation, with the Perdew-Burke-Ernzerhof (PBE) functional[24] for electron exchange and correlation potentials, as implemented in the VASP code.[25] The electron-ion interaction was described by the projector augmented wave (PAW) method,[26] and the energy cutoff was set to 400 eV. A 5×5 BN supercell including one single-vacancy or C impurity was used in our calculations. Our test calculations on 7×7 supercell gave the same defect configurations and defect levels. The structures were fully optimized using the conjugate gradient algorithm until the residual atomic forces to be smaller than 10 meV/Å. A Γ-centered 6×6 *k*-point sampling was used for the Brillouin-zone integration. The supercell with periodic boundary conditions was adopted to model the BN structures, with a vacuum layer larger than 10 Å to eliminate the interaction between the defects in the neighboring cells.

It is known that normal GGA type calculations usually underestimate the band gaps of semiconductors and the absolute band edge energy from the GGA calculation is not always reliable.[27] Since hybrid functional calculations can give improved results for semiconductors, we also adopt HSE hybrid functional[28,29] to calculate the band structures and defect formation energies in single-layer BN. For the calculations of defects in bilayer and bulk *h*-BN, the effect of

 ©2012 American Physical Society

van de Waals (vdW) interactions is taken into account by using the empirical correction scheme of Grimme (DFT + D),[30] which has been proven to be successful in describing the geometries of layered structures.[30–32] The interlayer distance of *h*-BN under DFT + D calculation is 6.17 Å, very consistent with previous results.[31]

The formation energies $\Delta H_f(\alpha,q)$ of defects are calculated as follows:[33]

$$\Delta H_f(\alpha,q) = \Delta E(\alpha,q) + \sum n_i\mu_i + qE_F \quad (1)$$

where

$$\Delta E(\alpha,q) = E(\alpha,q) - E\,(\text{host}) + \sum n_i E\,(i) + q\varepsilon_{VBM}\,(\text{host}). \quad (2)$$

$E(\alpha,q)$ is the total energy for a host material containing defect α in charge state q. E (host) is the total energy of host material without the defect. E_F is referenced to the valence band maximum (VBM) of the host. μ_i is the chemical potential of constituent i referenced to elemental solid/gas with energy E (i). n_i is the number of elements and q is the number of electrons transferred from the supercell to the reservoirs in forming the defect cell.

When a BN sheet is in equilibrium, μ_B and μ_N should satisfy $\mu_B + \mu_N = \mu_{BN}$, where μ_{BN} is the total energy of a BN pair in a BN sheet. When we calculate the formation energies of C impurity in BN, μ_C is taken from graphene. The values of μ_B and μ_N are defined by the growth conditions. In this paper, we only show the formation energies of vacancy and C impurity under N-rich conditions, since N_2 is possible to exist if the vacuum condition is imperfect during the synthesis of BN layers.

III. RESULTS AND DISCUSSION

A. Pristine single-layer BN

Single-layer BN is an indirect semiconductor and the band gap under PBE calculation is 4.56 eV, as shown in Fig. 1(a), agreeing with previous calculations.[34,35] The edge of valence bands is contributed by the P_z orbitals of N atoms. The CBM at Γ point is the nearly-free-electron (NFE) state with a maximum charge density at about 2 Å away from the BN plane,[34] as shown in Fig. 1(c). The calculated electron effective mass at NFE state is around 1 m_e and this value changes slightly along the different planar directions. It has been shown that the NFE state generally exists in isolated crystalline sheets and nanotubes.[34,36,37] Since this NFE state is not contributed to by B and N atoms, the neutral defects in the BN layer have little effect on it. However, the NFE state can be quite sensitive to the crystal potential averaged over the plane parallel to the BN layer,[38,39] thus it is expected that the charged defects could have large effect on its energy level, as we found in the following sections.

The band gap of BN in experiment is around 6 eV;[10,11] obviously, the PBE calculation underestimates the band gap of BN, as usually found in wide band-gap semiconductors. The more accurate HSE functional calculation provides a gap of 5.56 eV, as shown in Fig. 1(b), in good agreement with that from quasiparticle GW calculations.[34] The valence band structures obtained from HSE calculations are quite consistent

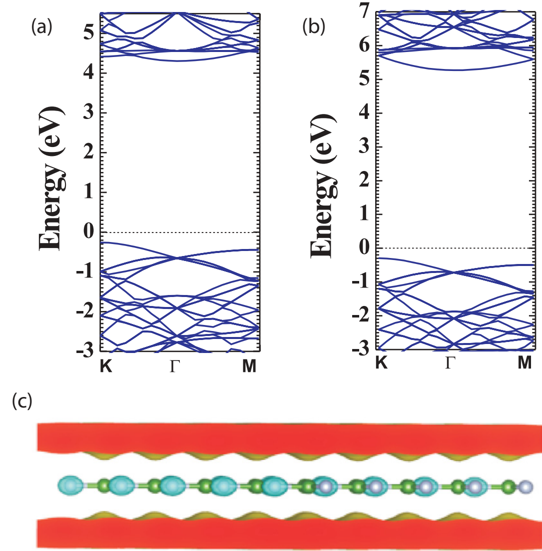

FIG. 1. (Color online) (a) The PBE-calculated band structure of pristine 5 × 5 BN. (b) The HSE-calculated band structure of pristine 5 × 5 BN. The Fermi level is set to zero. (c) The side view of Γ-point wave functions at the CBM of BN.

with that from PBE calculations, as shown in Figs. 1(a) and 1(b). The inclusion of Hartree-Fock exchange in HSE calculations has significant effects on the absolute energy scale of both VBM and CBM, which is mainly contributed by the respective anion and cation in ionic semiconductors. Since the NFE state is not contributed by the B or N atoms, it is expected that the effect of HSE correction on NFE state is much smaller than other conduction bands. As a result, the NFE state at the CBM becomes even lower in energy compared to other conduction bands in HSE calculation, as shown in Fig. 1(b).

B. Single boron vacancy in single-layer BN

Single boron vacancy (V_B) exists as a dominate defect during the fabrication of single-layer BN via electron beam irradiation in experiments.[4,5] The optimized local structure of V_B is shown in Fig. 2(a). After relaxation, it is found that Jahn-Teller distortion lowers its local symmetry from D_{3h} to C_{2v}, which is consistent with the fact that the three nearest N-N bond lengths at the vacancy are not equal, as shown in Fig. 2(a). The magnetic moments of N atoms at the vacancy are 1, 1, and −1 μ_B, respectively. The N-N distance between the two N atoms at V_B with opposite spin direction is ∼2.70 Å while the distance between the two N atoms with the same spin direction is increased to ∼2.78 Å due to Coulomb repulsion.

The PBE-calculated band structure of V_B is shown in Fig. 2(b). Because of the exchange splitting of the half and unoccupied states, Jahn-Teller effect results in the double-degenerate defect levels in the gap splitting into two single defect levels. One single defect level in the spin-up channel is even pushed down into the valence band. Finally, there is (are) one (two) unoccupied defect level(s) above the VBM in the spin-up (spin-down) channel, as marked by 1, 2, and 3 in Fig. 2(b). The energy difference between the defect levels and VBM are 0.5, 0.5, and 1.2 eV for levels 1, 2, and 3, respectively, agreeing with previous calculations.[22] From

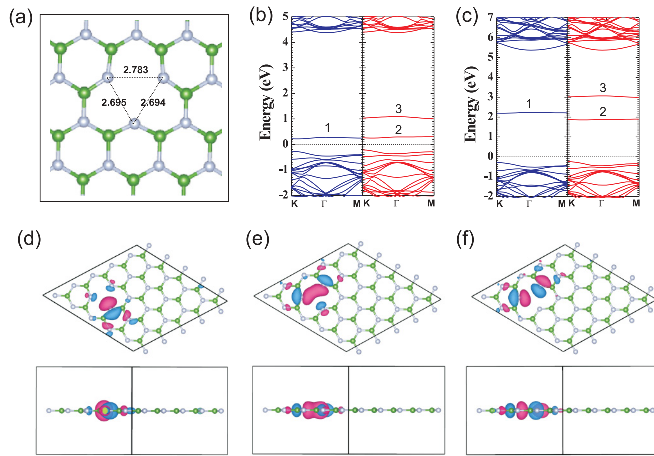

FIG. 2. (Color online) (a) The top view of optimized local structure of V_B. The N-N bond lengths at the vacancy are also shown in this figure. (b) The PBE-calculated spin-polarized band structure of V_B. (c) The HSE-calculated spin-polarized band structure of V_B. The Fermi level is set to zero. (d), (e), (f) are the top view and side view of Γ-point wave functions of the defect levels marked as 1, 2, and 3 in (b), respectively.

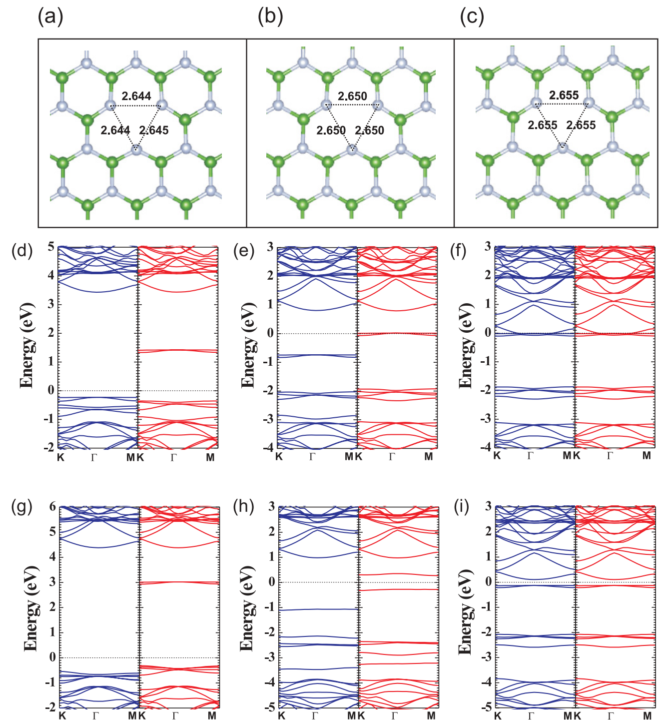

FIG. 3. (Color online) (a) The top view of optimized local structure of (a) V_B^{-1}, (b) V_B^{-2}, and (c) V_B^{-3}. The N-N bond lengths at the vacancy are also shown in this figure. The PBE-calculated spin-polarized band structure of (d) V_B^{-1}, (e) V_B^{-2}, and (f) V_B^{-3}. The HSE-calculated spin-polarized band structure of (g) V_B^{-1}, (h) V_B^{-2}, and (i) V_B^{-3}. The Fermi level is set to zero.

the corresponding wave functions of these three defect levels [Figs. 2(d)–2(f)], we see that all the defect levels are σ-type, originated from the P_x and P_y orbitals of N atoms at the vacancy. After band-gap correction by the HSE calculations, the three in-gap defect levels become much deeper, as shown in Fig. 2(c). The energy differences between the defect levels and VBM are 2.5, 2.1, and 3.2 eV for levels 1, 2, and 3, respectively. Usually, the defect levels in semiconductors (e.g., ZnO) gotten from HSE calculations are deeper than those gotten from LDA/GGA-type calculations, which is mainly because the absolute energy of VBM (or CBM) is pushed down (or up) compared to PBE calculations.[40] Although it is known that HSE calculations could give improved band gaps for semiconductors, there is still no definite evidence that the relative positions of defect levels gotten from HSE calculations are always more reasonable than PBE calculations. Thus, we are trying to exhibit both PBE and HSE results of all the defects for comparison. The wave functions of these defect levels under HSE calculations are almost the same as under PBE calculations.

Since there are three unoccupied defect levels in the band gap of V_B, it is expected that the possible charge states of V_B can range from 0 to −3. The optimized charged defect structures are shown in Figs. 3(a)–3(c). When V_B is in −1 charge state (V_B^{-1}), its local symmetry changes from C_{2v} to D_{3h}, and the three N-N bond lengths at the vacancy decrease to ∼2.644 Å, as shown in Fig. 3(a). This kind of defect reconstruction lowers the total energy of V_B^{-1} by ∼400 meV. The local symmetry of V_B^{-2} and V_B^{-3} is similar to that of V_B^{-1}, but the N-N bond lengths at the vacancy are increased to 2.650 and 2.655 Å, respectively, due to the increased Coulomb repulsion between these negative charged N atoms at the vacancy site.

The PBE-calculated band structures of V_B^{-1}, V_B^{-2}, and V_B^{-3} are shown in Figs. 3(d)–3(f). Because the defect symmetry is changed to D_{3h}, the configurations of defect levels are also changed. Under D_{3h} symmetry there are five (six) defect levels that appear in the band gap in the spin-up (spin-down) channel, which is more complicated than the neutral case with C_{2v} symmetry. Three of them in lower energies are π-type defect levels (contributed by the P_z orbitals of N atoms at the vacancy), and the remaining two (three) in higher energies in the spin-up (spin-down) channel are σ-type. For V_B^{-1} [Fig. 3(d)], only the two σ-type defect levels in the spin-down channel are unoccupied, giving rise to a total magnetic moment of 2 μ_B. Since the NFE state at CBM is very weakly bound to the BN surface, its charge density is unusually facile and can adapt easily to the changes in the self-consistent electrostatic potential. Thus, the NFE state is pulled down (up) rapidly when the system is negatively (positively) charged due to the universal electrostatic mechanism,[38,39] as shown in Fig. 3.

When one more electron is added to one of the two unoccupied σ-type levels of V_B^{-1} to form V_B^{-2} [Fig. 3(e)], the defect levels shift up in energy due to Coulomb repulsion between the occupied electrons. Again, when one more electron is added to V_B^{-2} to form V_B^{-3}, because the defect levels are further shifted up and the NFE state is dropped down, finally the defect level is even above the NFE state, which makes the NFE state partially occupied. Clearly, it is not possible to fully realize V_B^{-3} (under the PBE calculations). Our test calculations on a larger supercell give the same conclusion. When an extra hole is added to V_B, the defect symmetry and in-gap levels are the same as V_B^0, thus the added hole occupies

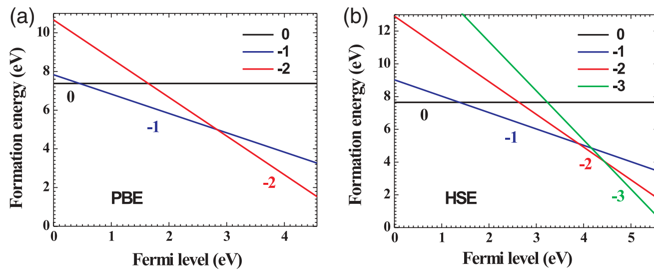

FIG. 4. (Color online) (a) The V_B formation energies as a function of electron Fermi level under PBE calculations in N-rich conditions. (b) The V_B formation energies as a function of electron Fermi level under HSE calculations in N-rich conditions.

the valence bands rather than defect levels and V_B^{+1} cannot be achieved.

The HSE-calculated band structures of V_B^{-1}, V_B^{-2}, and V_B^{-3} are shown in Figs. 3(g)–3(i). The occupation of defect levels in -1 and -2 charge states is similar to that gotten from PBE calculations except that the half-occupied defect levels, which are almost degenerate in PBE calculation [Fig. 3(e)], now is split into fully occupied and unoccupied levels [Fig. 3(h)] due to the enhanced exchange-splitting effect in HSE calculations. An obvious difference between PBE and HSE results is found for the case of V_B^{-3}. Under PBE calculation V_B cannot fully realize a -3 charge state but it is opposite for HSE calculation, as shown in Fig. 3(i).

The PBE- and HSE-calculated formation energies of V_B are shown in Fig. 4. The formation energies of V_B^0 under PBE and HSE calculations are 7.38 and 7.65 eV, respectively, indicating that PBE is good enough for calculating the formation energy of neutral V_B^0. Moreover, the formation energy of V_B^0 in the BN sheet is larger than that in the BN nanotube,[20] which is mainly because the bendinglike deformations in the BN nanotube can reduce the formation energy of defects. The respective defect energy transition levels of $0/-1$ and $-1/-2$ are 0.44 and 2.83 eV with respect to VBM under PBE calculations. Under HSE calculations, as shown in Fig. 4(b), the transition levels of $0/-1$ and $-1/-2$ become much deeper and are 1.35 and 3.89 eV above VBM, respectively. This is consistent with the band structure calculations in Fig. 3.

C. Single nitrogen vacancy in single-layer BN

Nitrogen vacancy (V_N) has also been demonstrated to exist in h-BN in experiments.[2,6,12,13] Differing from V_B, there is no obvious structural distortion after the structural relaxation of V_N and the defect symmetry is D_{3h}. The nearest B-B bond lengths at V_N are the same (~2.31 Å), as shown in Fig. 5(a), consistent with other calculations.[17,18,20,22] The magnetic moments of N atoms at vacancy are equal to each other and contribute to a total magnetic moment of 1 μ_B. The PBE-calculated band structure of V_N is shown in Fig. 5(b). There is one single gap level (marked as 1) and two mostly degenerated gap levels (marked as 2 and 3) in each spin channel. Level 1 is π-type while levels 2 and 3 are σ-type, as shown in Figs. 5(d)–5(f). Only level 1 in the spin-up channel is occupied and levels 2 and 3 are close to the CBM. The energy difference between level 1 in the spin-up (spin-down)

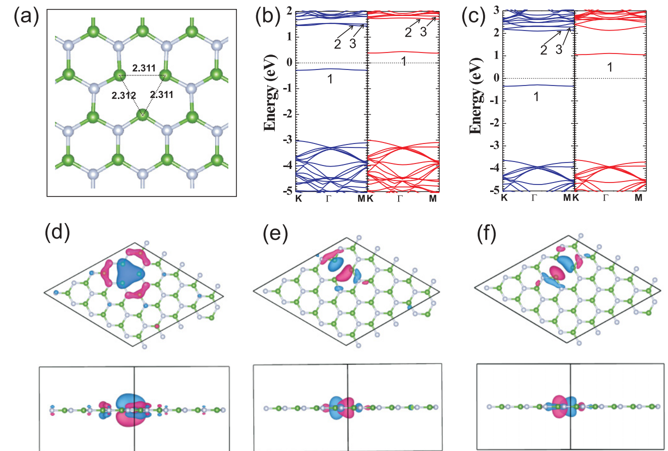

FIG. 5. (Color online) (a) The top view of optimized local structure of V_N. The B-B bond lengths at the vacancy are also shown in this figure. (b) The PBE-calculated spin-polarized band structure of V_N. (c) The HSE-calculated spin-polarized band structure of V_N. The Fermi level is set to zero. (d), (e), (f) are the top view and side view of Γ-point wave functions of the defect levels marked as 1, 2, and 3 in (b), respectively.

channel and VBM is 2.74 (3.39) eV. The HSE-calculated band structure of V_N is shown in Fig. 5(c). Level 1 becomes deeper and the energy difference between level 1 in the spin-up (spin-down) channel and VBM is 3.29 (4.68) eV. Levels 2 and 3 in the spin-up (or spin-down) channel are even more close to the CBM (or above the CBM) in HSE calculations because of the increased exchange-splitting effect in HSE calculations.

The possible charge states of V_N range from -3 to $+1$ by simply counting the possible occupation of defect levels. For the case of V_N^{-1}, the B-B bond lengths at the vacancy decrease from 2.31 to 2.10 Å [Fig. 6(a)]. Comparing to V_N^0, the unoccupied defect level 1 in the spin-down channel is now occupied and the system becomes spin-unpolarized, as shown in Fig. 6(c). Due to the downshift of the NFE state in negative charged BN, the defect levels 2 and 3 are now above the NFE state in energy. More excess electrons will be added to the NFE state rather than the defect state. Thus, the highest negative charged states of V_N can not be less than -1. Since there is only one occupied defect level in the spin-up channel, the possible positive charged state cannot exceed $+1$. For the case of V_N^{+1}, as shown in Fig. 6(d), the occupied level 1 in the spin-up channel is now unoccupied and the system is spin-unpolarized. Due to the upshift of NFE state in positive charged BN, the defect levels 2 and 3 becomes deeper compared to CBM. The HSE-calculated band structures of V_N^{-1} and V_N^{+1} are similar to that of PBE-calculated results, as shown in Figs. 6(e) and 6(f).

The PBE and HSE calculated formation energies of V_N are shown in Fig. 7. The formation energy of V_N^0 is 7.70 eV, which is 0.77 eV lower than that gotten from HSE calculation. The transition energy levels of $0/+1$ and $0/-1$ are 2.58 and 3.16 eV with respect to VBM, indicating that the defect levels are too deep to be ionized. These deep levels of V_N have a big influence on the luminescence of BN.[2,6,12,13] Under HSE calculations, the transition energy levels of $0/+1$ and $0/-1$ are 3.56 and 4.17 eV above VBM. Interestingly, the energy level

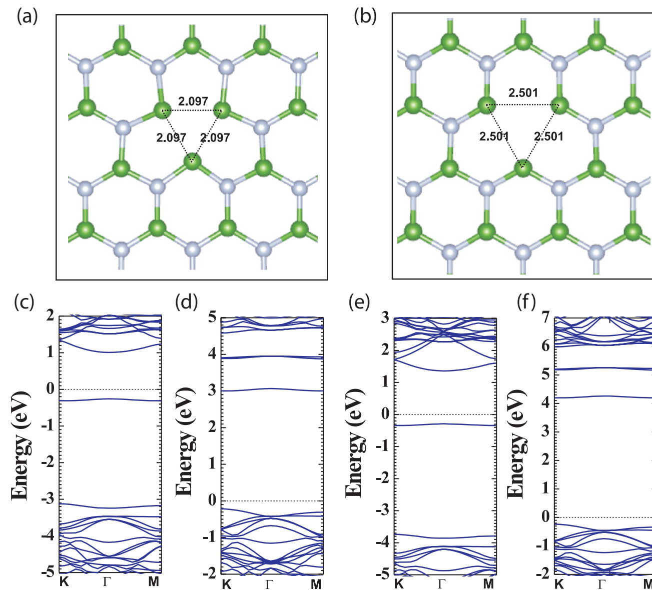

FIG. 6. (Color online) (a) The top view of optimized local structure of (a) V_N^{-1} and (b) V_N^{+1}. The B-B bond lengths at the vacancy are also shown in this figure. The PBE-calculated spin-unpolarized band structure of (c) V_N^{-1} and (d) V_N^{+1}. The HSE-calculated spin-unpolarized band structure of (e) V_N^{-1} and (f) V_N^{+1}. The Fermi level is set to zero.

of $0/+1$ (or $0/-1$) with respect to CBM is similar for both PBE and HSE calculations, agreeing with the band structures shown in Fig. 6.

D. Carbon substitutional of boron in single-layer BN

Carbon is a common impurity in BN, as found in lots of experiments.[2,6,12,13] Thus, a full understanding of the defect properties of C substitutional of B (C_B) or N (C_N) is of great importance. Since the valence electrons between B (N) and C is only one, it is expected that the defect levels induced by C_B or C_N are more simple than vacancies. The symmetry of C_B is D_{3h} and the optimized C_B structure is shown in Fig. 8(a). The C-N bond length is 1.409 Å, shorter than that of B-N (1.451 Å), which is because of the smaller atomic size of C than B. Because C is more electronegative than B, there is a defect level [level 1 marked in Figs. 8(b) and 8(c)] pull down from the conduction band and it is occupied (unoccupied) in the spin-up (spin-down) channel. This defect level 1 is contributed by the P_z orbitals of C and its neighbor B and N atoms, as shown in Fig. 8(d). The energy difference between level 1 in the spin-up (spin-down) channel and VBM is 3.40 (4.29) eV. Under HSE calculation, the exchange splitting energy between occupied level 1 in the spin-up channel and unoccupied level 1 in the spin-down channel is even larger, as shown in Fig. 8(c), which push the occupied (unoccupied) defect level in lower (higher) energy. The unoccupied level 1 in the spin-down channel is even pushed up higher than the NFE state. The energy difference between level 1 in the spin-up channel and VBM is 3.74 eV, slightly larger than that gotten from PBE calculation.

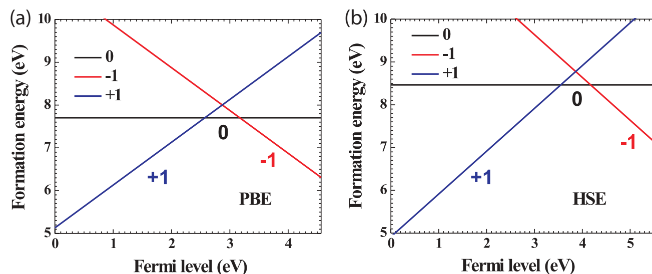

FIG. 7. (Color online) (a) The V_N formation energies as a function of electron Fermi level under PBE calculations in N-rich conditions. (b) The V_N formation energies as a function of electron Fermi level under HSE calculations in N-rich conditions.

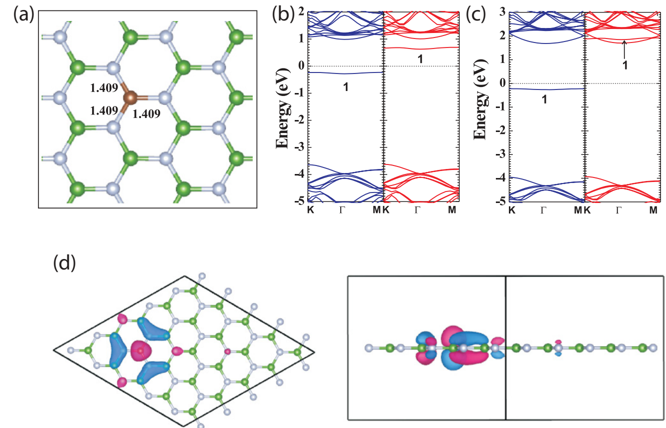

FIG. 8. (Color online) (a) The top view of optimized local structure of C_B. The C-N bond lengths are shown in this figure. (b) The PBE-calculated spin-polarized band structure of C_B. (c) The HSE-calculated spin-polarized band structure of C_B. The Fermi level is set to zero. (d) The top view and side view of Γ-point wave functions of the defect levels marked as 1 in (b).

Since there is only one defect level in the band gap of C_B, the possible charge states of C_B may range from -1 to $+1$. Different from vacancy defects, the structural relaxation effect for C impurity in its charged states is smaller, as shown in Figs. 9(a) and 9(b). The C-N bond length around the defect is 1.41 (1.38) Å when one excess electron (hole) is induced to C_B. When one excess electron is added to C_B^0, the NFE state is downshift and the defect level 1 is pushed up due to the Coulomb repulsion between the occupied electrons. Finally, the defect level is even above CBM and the additional electron is added to the NFE state, as shown in Figs. 9(c) and 9(e). Thus C_B^{-1} cannot be realized although there is an unoccupied level 1 in C_B^0. When one excess hole is added to the defect level of C_B^0, the original occupied defect level 1 in the spin-up channel becomes occupied and the system is now spin-unpolarized, as shown in Figs. 9(d) and 9(f). The occupied level 1 is shifted down a little while the NFE state is upshifted significantly. Our above defect calculations demonstrate that C_B can only realize $+1$ charge state.

As shown in Fig. 10, the PBE and HSE calculated formation energies of C_B^0 are quite close to each other (PBE: 1.68 eV, HSE: 1.76 eV). The formation energy of C_B is quite small compared to that of vacancies (Figs. 4 and 7). The transition

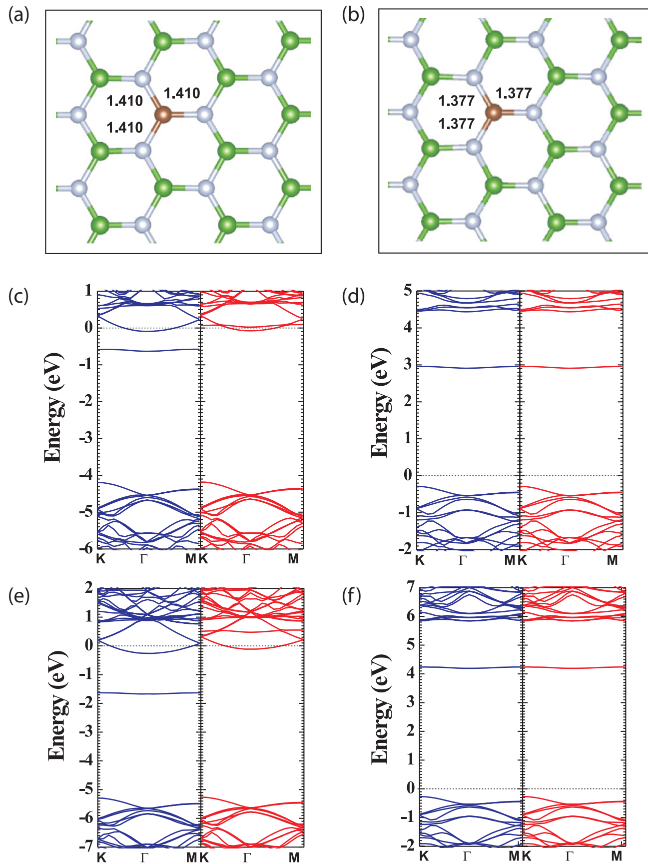

FIG. 9. (Color online) (a) The top view of optimized local structure of (a) C_B^{-1} and (b) C_B^{+1}. The C-N bond lengths are also shown in this figure. The PBE-calculated band structure of (c) C_B^{-1} and (d) C_B^{+1}. The HSE-calculated band structure of (e) C_B^{-1} and (f) C_B^{+1}. The Fermi level is set to zero.

energy level of $0/+1$ is 3.01 and 3.82 eV with respect to CBM in PBE and HSE calculations, respectively, indicating that the defect level of C_B is quite deep. It also agrees with the experimental observations that C impurity has significant influence on the luminescence of BN.[2,6,12,13]

E. Carbon substitutional of nitrogen in single-layer BN

The relaxed structure of C_N is shown in Fig. 11(a). The symmetry of C_N is D_{3h} and the C-B bond length is 1.509 Å,

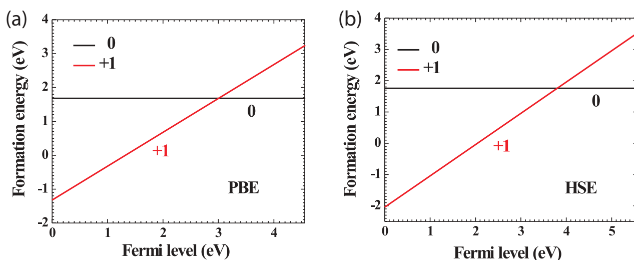

FIG. 10. (Color online) (a) The C_B formation energies as a function of electron Fermi level under PBE calculations. (b) The C_B formation energies as a function of electron Fermi level under HSE calculations.

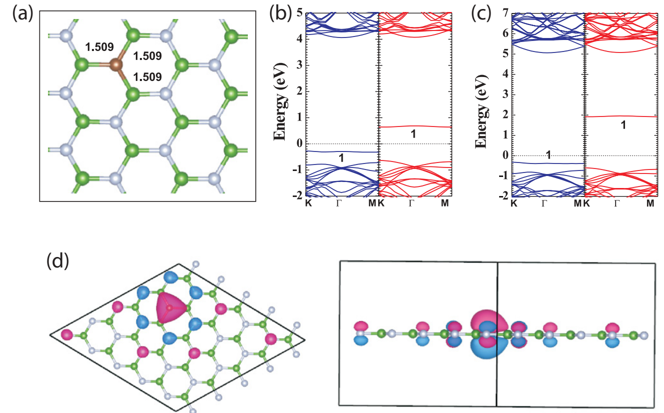

FIG. 11. (Color online) (a) The top view of optimized local structure of C_N. The C-B bond lengths are shown in this figure. (b) The PBE-calculated spin-polarized band structure of C_N. (c) The HSE-calculated spin-polarized band structure of C_N. The Fermi level is set to zero. (d) The top view and side view of Γ-point wave functions of the defect levels marked as 1 in (b).

larger than that of BN (1.451 Å), mainly due to the larger atomic size of C than N. Since the valence electrons of C is one less than that of N, there is a defect level (level 1) originated from the valence band in the band gap. Level 1 is occupied (unoccupied) in the spin-up (spin-down) channel, as shown in Figs. 11(b) and 11(c). The energy difference between level 1 in spin-up (spin-down) channel and VBM is 0.44 (1.28) eV. The plotted wave functions of level 1 is shown in Fig. 11(d). The defect level of C_N is contributed by the P_z orbitals of C and its adjacent N atoms. The exchange splitting energy of defect level 1 under HSE calculation is much larger than under PBE calculation, as shown in Fig. 11(c). The energy difference between level 1 in spin-up (spin-down) channel and VBM is 0.41 (2.51) eV.

Similar to that of C_B, the possible charge states of C_N range from $+1$ to -1. The optimized structures and related band structures of C_N^{-1} and C_N^{+1} are shown in Fig. 12. The C-B bond lengths decrease (increase) from 1.51 Å to 1.47 (1.52) Å for C_N^{-1} (C_N^{+1}). The defect level 1 can be fully occupied or unoccupied and the system becomes spin-unpolarized when one additional electron or hole is induced to C_N^0, as shown in Fig. 12. More excess electrons or holes will be added to CBM and VBM, respectively.

The calculated formation energies of C_N as a function of electron Fermi level are shown in Fig. 13. Generally, the $+1$ charge state is not stable, and the energy transition level $0/-1$ is 1.44 and 2.24 eV with respect to CBM for PBE and HSE calculations, respectively, which is consistent with other defect cases that hybrid calculations give deeper transition energy levels compared to that of GGA calculations.

F. Layer effect on the defect properties of *h*-BN

All the above discussions are focused on the defects in single-layer BN, and one interesting issue is to investigate the layer effect on the structural and electronic properties of defects in BN. Here, we select V_B defect in bilayer and bulk BN as examples to demonstrate the layer effect. The (ground

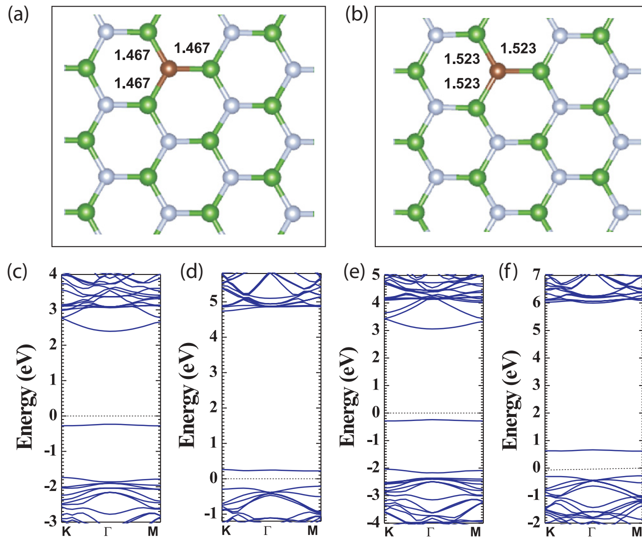

FIG. 12. (Color online) (a) The top view of optimized local structure of (a) C_N^{-1} and (b) C_N^{+1}. The C-B bond lengths are also shown in this figure. The PBE-calculated spin-unpolarized band structure of (c) C_N^{-1} and (d) C_N^{+1}. The HSE-calculated spin-unpolarized band structure of (e) C_N^{-1} and (f) C_N^{+1}. The Fermi level is set to zero.

state) AB stacking sequence with each boron atom on top of a nitrogen atom is considered. For the case of V_B^0, the defect symmetry and the N-N bond lengths at the vacancy in bilayer and bulk BN are quite similar to that of single-layer BN (Fig. 2). Surprisingly, the situation is quite different for highest charge state $q = -3$, as shown in Figs. 14(a) and 14(b). When the three N atoms around the vacancy are highly negatively charged, the Coulomb interaction between N atoms at the vacancy and the B atoms in its adjacent layer is largely enhanced, which finally leads to the interlayer BN bonds, as shown in Figs. 14(a) and 14(b). The interlayer BN bond lengths for bilayer layer and bulk are 1.71 and 1.64 Å, respectively. The forming of interlayer BN bonds in bilayer BN has been observed in a recent experiment.[41]

The PBE-calculated formation energies of possible charge states of V_B in bilayer and bulk BN are shown in Figs. 14(c) and 14(d). Due to the large supercell of bilayer and bulk *h*-BN, HSE calculations are too expensive to be carried out. The formation energies of V_B^0 in bilayer and bulk BN are similar to that in single-layer BN. Differing from single-layer BN, the NFE state is absent at the bottom of conduction bands in

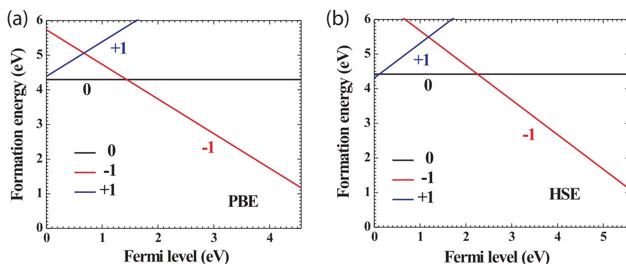

FIG. 13. (Color online) (a) The C_N formation energies as a function of electron Fermi level under PBE calculations. (b) The C_N formation energies as a function of electron Fermi level under HSE calculations.

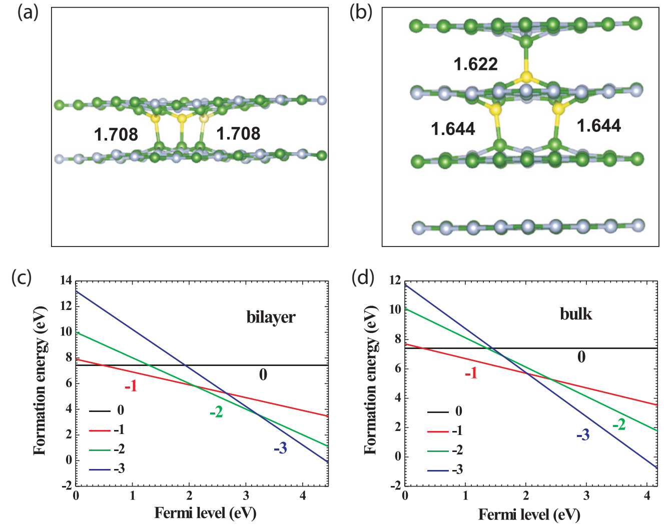

FIG. 14. (Color online) The side view of optimized structures of V_B^{-3} in (a) bilayer and (b) bulk BN. The interlayer BN bond lengths are shown in these figures. (b) The PBE-calculated formation energies V_B^{-3} in (c) bilayer and (d) bulk BN as a function of electron Fermi level.

bilayer and bulk BN,[34] thus the V_B^{-3} state can be realized even under PBE calculations. Differing from bilayer and single-layer BN, the V_B^{-2} charge state is not stable for bulk BN in the whole chemical potential range, as shown in Fig. 14(d). Our calculated formation energies and transition energy levels of V_B in bulk BN are different from a previous report where V_B^0 is shown to be always less stable than charge state (i.e., negative U),[16] which may be because the spin-polarization effect of V_B is not considered. Also, the interlayer bonds[41] are not observed in their calculations.

IV. CONCLUSION

By using both normal GGA and HSE calculations, we have systematically calculated the vacancy defects and C impurity properties in BN. It is found that the defect configurations and the local bond lengths around defects are quite sensitive to their charge states. Interestingly, the highest negative charge states of defects are largely determined by the NFE state at CBM. The in-gap defect levels gotten from hybrid functional calculations are quite deeper than those gotten from GGA calculations. The formation energies of neutral defects calculated by HSE and GGA are close to each other, but the transition energy levels are quite different under GGA and HSE calculations. Finally, we show that the charged defect configurations as well as the transition energy levels exhibit interesting layer effects.

ACKNOWLEDGMENTS

B.H. thanks the helpful discussions with Dr. Su-Huai Wei and Dr. Qiang Xu. H.L. was supported by the WCU Program (Grant No. R31-2008-000-10057-0), and by the Basic Science Research Program (Grant No. KRF-2012R1A1A1013124) through the National Research Foundation of Korea, funded by the Ministry of Education, Science and Technology. The authors also acknowledge the support from KISTI under the Supercomputing Applications Support Program (KSC-2012-C2-52).

*Current address: National Renewable Energy Laboratory, Colorado 80401, USA; bing.huang@nrel.gov
†hkiee3@konkuk.ac.kr

[1] *Synthesis and Properties of Boron Nitride*, edited by J. J. Pouch and S. A. Alteroviz (Trans Tech, Switzerland, 1990).
[2] K. Watanabe, T. Taniguchi, and H. Kanda, Nat. Mater. **3**, 404 (2004).
[3] B. Arnaud, S. Lebegue, P. Rabiller, and M. Alouani, Phys. Rev. Lett. **96**, 026402 (2006).
[4] C. Jin, F. Lin, K. Suenaga, and S. Iijima, Phys. Rev. Lett. **102**, 195505 (2009).
[5] J. C. Meyer, A. Chuvilin, G. Algara-Siller, J. Biskupek, and U. Kaiser, Nano Lett. **9**, 2683 (2009).
[6] Y. Kubota, K. Watanabe, O. Tsuda, and T. Taniguchi, Science **317**, 932 (2007).
[7] K. S. Novoselov, D. Jiang, F. Schedin, T. J. Booth, V. V. Khotkevich, S. V. Morozov, and A. K. Geim, Proc. Natl. Acad. Sci. USA **102**, 10451 (2005).
[8] O. L. Krivanek, M. F. Chisholm, V. Nicolosi, T. J. Pennycook, G. J. Corbin, N. Dellby, M. F. Murfitt, C. S. Own, Z. S. Szilagyi, M. P. Oxley, S. T. Pantelides, and S. J. Pennycook, Nature (London) **464**, 571 (2010).
[9] W. Auwarter, H. U. Suter, H. Sachdev, and T. Greber, Chem. Mater. **16**, 343 (2004).
[10] Y. Shi, C. Hamsen, X. Jia, K. K. Kim, A. Reina, M. Hofmann, A. L. Hsu, K. Zhang, H. Li, Z.-Y. Juang, M. S. Dresselhaus, L.-J. Li, and J. Kong, Nano Lett. **10**, 4134 (2010).
[11] L. Song, L. Ci, H. Lu, P. B. Sorokin, C. Jin, J. Ni, A. G. Kvashnin, D. G. Kvashnin, J. Lou, B. I. Yakobson, and P. M. Ajayan, Nano Lett. **10**, 3209 (2010).
[12] M. G. Silly, P. Jaffrennou, J. Barjon, J.-S. Lauret, F. Ducastelle, A. Loiseau, E. Obraztsova, B. Attal-Tretout, and E. Rosencher, Phys. Rev. B **75**, 085205 (2007).
[13] L. Museur, E. Feldbach, and A. Kanaev, Phys. Rev. B **78**, 155204 (2008).
[14] L. Ci, L. Song, L. Jin, D. Jariwala, D. Wu, Y. Li, A. Srivastava, Z. F. Wang, K. Storr, L. Balicas, F. Liu, and M. A. Ajayan, Nat. Mater. **9**, 430 (2010).
[15] X. Wei, M. Wang, Y. Bando, and D. Golberg, ACS Nano **5**, 2916 (2011).
[16] W. Orellana and H. Chacham, Phys. Rev. B **63**, 125205 (2001).
[17] M. S. Si and D. S. Xue, Phys. Rev. B **75**, 193409 (2007).
[18] R.-F. Liu and C. Cheng, Phys. Rev. B **76**, 014405 (2007).
[19] S. Okada, Phys. Rev. B **80**, 161404 (2009).
[20] S. Azevedo, J. R. Kaschny, C. M. C. de Castilho, and F. de BritoMota, Eur. Phys. J. B **67**, 507 (2009).
[21] L.-C. Yin, H.-M. Cheng, and R. Saito, Phys. Rev. B **81**, 153407 (2010).
[22] C. Attaccalite, M. Bockstedte, A. Marini, A. Rubio, and L. Wirtz, Phys. Rev. B **83**, 144115 (2011).
[23] N. Berseneva, A. V. Krasheninnikov, and R. M. Nieminen, Phys. Rev. Lett. **107**, 035501 (2011); B. Huang and S.-H. Wei, *ibid.* **107**, 239601 (2011).
[24] J. P. Perdew, K. Burke, and M. Ernzerhof, Phys. Rev. Lett. **77**, 3865 (1996).
[25] G. Kresse and J. Furthmüller, Comput. Mater. Sci. **6**, 15 (1996).
[26] G. Kresse and D. Joubert, Phys. Rev. B **59**, 1758 (1999).
[27] A. Alkauskas, P. Broqvist, F. Devynck, and A. Pasquarello, Phys. Rev. Lett. **101**, 106802 (2008).
[28] J. Heyd, G. E. Scuseria, and M. Ernzerhof, J. Chem. Phys. **118**, 8207 (2003).
[29] J. Heyd, G. E. Scuseria, and M. Ernzerhof, J. Chem. Phys. **124**, 219906 (2006).
[30] S. Grimme, J. Comput. Chem. **27**, 1787 (2006).
[31] T. Bucko, J. Hafner, S. Lebegue, and J. G. Angyan, J. Phys. Chem. A **114**, 11814 (2010).
[32] B. Huang, Q. Xu, and S.-H. Wei, Phys. Rev. B **84**, 155406 (2011).
[33] S.-H. Wei, Comput. Mater. Sci. **30**, 337 (2004).
[34] X. Blase, A. Rubio, S. G. Louie, and M. L. Cohen, Phys. Rev. B **51**, 6868 (1995).
[35] M. Topsakal, E. Akturk, and S. Ciraci, Phys. Rev. B **79**, 115442 (2009).
[36] M. Posternak, A. Baldereschi, A. J. Freeman, E. Wimmer, and M. Weinert, Phys. Rev. Lett. **50**, 761 (1983).
[37] S. Okada, A. Oshiyama, and S. Saito, Phys. Rev. B **62**, 7634 (2000).
[38] E. R. Margine and V. H. Crespi, Phys. Rev. Lett. **96**, 196803 (2006).
[39] S. Hu, J. Zhao, Y. Jin, J. Yang, H. Petek, and J. G. Hou, Nano Lett. **10**, 4830 (2010).
[40] *Advanced Calculations for Defects in Materials: Electronic Structure Methods*, edited by A. Alkauskas, P. Deak, J. Neuge-bauer, A. Pasquarello, and C. G. Van deWalle (Wiley, Weinheim, Germany, 2011).
[41] N. Alem, O. V. Yazyev, C. Kisielowski, P. Denes, U. Dahmen, P. Hartel, M. Haider, M. Bischoff, B. Jiang, S. G. Louie, and A. Zettl, Phys. Rev. Lett. **106**, 126102 (2011).